PRAMANA
— journal of
physics

Vol. 85, No. 4
October 2015
pp. 723–737

Application of Tietz potential to study optical properties of spherical quantum dots

R KHORDAD* and B MIRHOSSEINI

Department of Physics, College of Sciences, Yasouj University, Yasouj 75914-353, Iran
*Corresponding author. E-mail: rezakh2025@yahoo.com

MS received 25 October 2013; revised 22 July 2014; accepted 21 August 2014
DOI: 10.1007/s12043-014-0906-3; ***e*Publication:** 18 June 2015

Abstract. In this work, we study the optical properties of spherical quantum dots by using Tietz potential. In this regard, we have applied Nikiforov–Uvarov (NU) technique and numerically solved the Schrödinger equation to obtain energy levels and wave functions. Then, by using the density matrix method, we have derived expressions for the changes in linear and third-order nonlinear absorption coefficients and refractive index. According to the results obtained from this work, it is deduced that: (i) the total refractive index and the absorption coefficients increase and shift towards higher energies as v_0 increases; (ii) the total absorption coefficient and refractive index decrease and also shift towards lower energies as r_0 increases.

Keywords. Quantum dot; refractive index change; linear and nonlinear optical properties; Tietz potential.

PACS Nos 73.21.Fg; 78.66.Fd; 78.67.De

1. Introduction

Of late, the studies on nanostructures have opened new fields in fundamental sciences. The physical properties of semiconductors such as optical, electronic, and thermodynamic properties have become the most essential and exciting in physics [1–3]. One of the most important points in the study of nanostructures is their preparation procedure. Hitherto, various procedures have been used for the preparation of nanostructures with controlled size, shape, and uniform size distribution [4–9].

Although semiconductor devices have fairly long history, the greatest developments in technology has occurred during the last two or three decades [10]. Low-dimensional systems have revolutionized semiconductor physics. In the past two decades, the investigation of semiconductor quantum-confined structures such as quantum wells, quantum wires, quantum rings, quantum dots etc., has gained considerable interest, because of their relevance in practical applications and as probes for the electronic structure of mesoscopic media [11–17].

The study and analysis of semiconductor quantum dots have always been of great importance both theoretically and experimentally. Quantum dots are exquisite tools by which quantum behaviour can be probed on a larger scale than the atomic, i.e., the nanometer scale. While the physics exhibited by these devices is closer to classical than to atomic physics, quantum dots are still sufficiently small to clearly exhibit quantum phenomena.

Recently, optical and electronic properties of semiconductors have attracted considerable attention in physics. Optical properties of quantum dots depend on both the size and composition of the dots. The linear and nonlinear optical properties have been studied theoretically by several researchers [18–24]. For example, Wang and Guo [18] investigated excitonic effects on the third-harmonic generation (THG) coefficient for typical GaAs/AlGaAs parabolic quantum dots. They obtained an analytic formula by using the compact-density-matrix approach and an iterative method. Recently, we have calculated the linear and nonlinear optical properties of T-shaped quantum wires [19]. Shao *et al* [20] investigated THG in cylindrical quantum dots with an applied electric field. Morales *et al* [21] calculated donor-related optical absorption spectra for a double quantum well under hydrostatic pressure and applied electric field. Karabulut *et al* [22] calculated the second- and third-harmonic generation susceptibilities of spherical quantum dots with parabolic confinement subjected to an external electric field in the presence of an impurity. The effect of pressure on intersubband optical absorption coefficients and changes in refractive index in a V-groove quantum wire was studied in [23]. Recently, in another work, we have studied the THG in GaAs/$Ga_{1-x}Al_xAS$ ridge quantum wires [24].

The aim of this paper is to study the intersubband absorption coefficients and the changes in refractive index in spherical quantum dots using Tietz potential. For this purpose, we have used the density matrix formulation to obtain the linear and third-order nonlinear changes in refractive index and absorption coefficients. First, we have solved the Schrödinger equation with Tietz potential to obtain wave functions and energy levels [25]. Then, we have obtained optical properties of this system. The paper is organized as follows: The total Hamiltonian of the system, relevant eigenvalues and wavefunctions are briefly presented in §2. Analytical expressions for the linear and nonlinear intersubband optical absorption coefficients and refractive index changes are presented in §3. The results and discussion are given in §4 and finally, conclusions are given in §5.

2. Theory and model

2.1 *Tietz potential*

It is well known that modelling the interaction potential of the real systems is of fundamental importance in many studies like atom–atom collisions, molecular spectroscopy, prediction of cluster structures, chemical reactivity, and transport properties of complex systems. Another application of the interaction potential is the long-lived metastable doubly or multiply charged ions that are relevant to high-density energy storage materials. Therefore, there is a great interest in searching for the interaction potential function of real systems. The reason is that the interaction potential function provides the most efficient way to summarize what we know about a system.

So far, many attempts have been done by researchers to analytically model the interaction potential function of real systems. The well-known potential functions are: Morse,

Born–Mayer, Hulburt–Hirschfelder, Rosen–Morse, Rydberg, Lennard–Jones, Wei, and Tietz potentials [26–30]. Some researchers have extended simple analytical potential functions and successfully used them in direct spectroscopic data fits for diatomic and polyatomic systems. For example, a modified Lennard–Jones potential, an expanded Morse potential, and an improved Tietz potential have been used for diatomic systems [31–33]. Among the aforementioned potential functions, the Tietz potential is an interesting case. The Tietz potential is given by

$$V(r) = V_0 \left(\frac{\sinh\left((r - r_0)/a\right)}{\sinh\left(r/a\right)} \right)^2, \tag{1}$$

where V_0 is the chemical potential of the electron gas and r_0 is the minimum value of the Tietz potential. The Tietz potential is more realistic than the Morse potential in describing the molecular dynamics at moderate and high rotation–vibrational quantum numbers [26,34]. The Tietz potential can be used to investigate the rotational–vibrational levels of diatomic molecules and zero-point vibrational corrections on the isotropic and anisotropic components of the hyperfine interaction. Liang *et al* [35] showed that the Tietz potential can be used to reproduce the interaction potential energy curve of the $A^1\Sigma_u^+$ state of Na_2. Recently, we investigated singlet–triplet transition of a two-electron quantum dot using the Tietz potential [36]. Our results showed much less transitions than the parabolic potential.

Some researchers have found that the deformed Rosen–Morse potential, Sun potential, and deformed four-parameter exponential-type potential are equivalent to the Tietz potential [37–39].

2.2 *Energy levels and wave functions*

In the framework of the effective-mass approximation, the Hamiltonian of an electron confined by a spherical quantum dot can be given as

$$H = -\frac{\hbar^2}{2m_e^*}\nabla^2 + V(r), \tag{2}$$

where m_e^* is the effective mass of the electron and $V(r)$ is the confining potential. In this work, we have considered the confining potential as the Tietz potential. To obtain energy levels and wave functions, it is required to solve the Schrödinger equation. With respect to eq. (1), the Schrödinger equation can be reduced to a radial equation which depends only on one coordinate.

Substituting the wave function in the form $\psi(r, \theta, \varphi) = R_{nl}(r)Y_l^m(\theta, \varphi)$ in the Schrödinger equation, the radial part of this equation is given by

$$\frac{\mathrm{d}^2 R_{nl}(r)}{\mathrm{d}r^2} + \frac{2}{r}\frac{\mathrm{d}R_{nl}(r)}{\mathrm{d}r} + \frac{2m_e^*}{\hbar^2} \times \left(E_{nl} - \frac{l\,(l+1)\,\hbar^2}{2m_e^* r^2} - V_0 \left(\frac{\sinh((r - r_0)/a)}{\sinh(r/a)} \right)^2 \right) R_{nl}(r) = 0, \tag{3}$$

where n and l are the principal and orbital quantum numbers. Also, E_{nl} are energy eigenvalues. Using the transformation $R_{nl} = U_{nl}(r)/r$, the radial eq. (3) appears as [25,40]

$$\frac{\mathrm{d}^2U_{nl}(r)}{\mathrm{d}r^2} = -\frac{2m_e^*}{\hbar^2}\{E_{nl} - V_0(\cosh(\alpha r_0) - \sinh(\alpha r_0)\coth(\alpha r_0))^2 - \frac{l(l+1)\hbar^2}{2m_e^* r^2}\}U_{nl}(r). \quad (4)$$

It is to be noted that there is no analytical solution for the above equation. Therefore, to solve the equation, a new improved approximation scheme (Pekeris-type approximation) is used for the centrifugal term as [41]

$$\frac{1}{r^2} \approx \frac{\alpha^2}{\sinh^2(\alpha r)} = \alpha^2\cosh^2(\alpha r), \quad (5)$$

where $\alpha = 1/a$. To check the above approximation, both sides of eq. (5) are plotted as a function of r in figure 1. Now, by substituting the centrifugal term in eq. (4) by eq. (5), one obtains

$$\frac{\mathrm{d}^2U_{nl}(r)}{\mathrm{d}r^2} + \frac{2m_e^*}{\hbar^2}\{E_{nl} - V_0\cosh^2(\alpha r_0) - V_0\sinh^2(\alpha r_0) - V_0\sinh^2(\alpha r_0)\mathrm{csch}^2(\alpha r) + 2V_0\cosh(\alpha r_0)\sinh(\alpha r_0)\coth(\alpha r) - \frac{l(1+1)\hbar^2\alpha^2}{2m_e^*}\}U_{nl}(r) = 0 \quad (6)$$

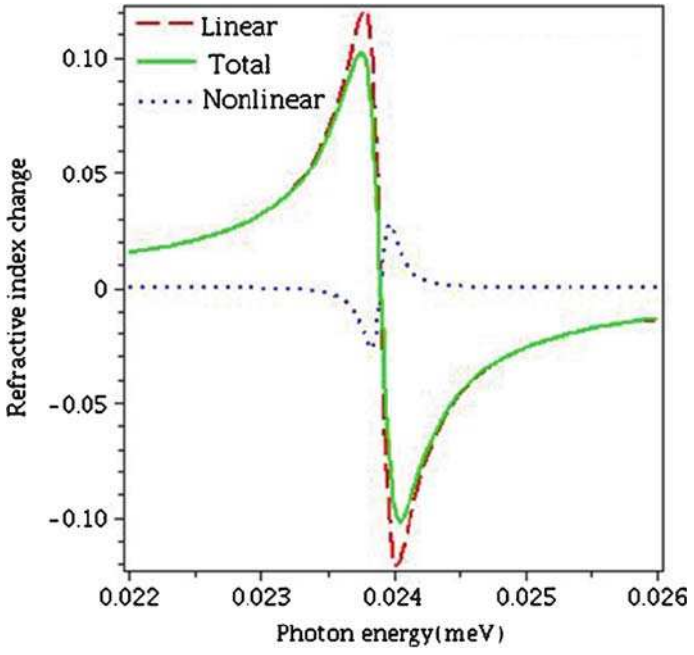

Figure 1. The linear, third-order nonlinear, and total refractive index changes as a function of photon energy for $\alpha = 0.01$, $m = 5\ \mathrm{fm}^{-1}$, $r_0 = 2$, and $v_0 = 0.2$.

or, alternatively

$$\frac{\mathrm{d}^2U_{nl}(r)}{\mathrm{d}r^2}+\left\{\frac{2m_{\mathrm{e}}^*}{\hbar^2}E_n-\frac{2m_{\mathrm{e}}^*V_0}{\hbar^2}\cosh^2(\alpha r_0)-\frac{2m_{\mathrm{e}}^*V_0}{\hbar^2}\sinh^2(\alpha r_0)\right.$$
$$-\frac{8m_{\mathrm{e}}^*V_0\sinh^2(\alpha r_0)\,\mathrm{e}^{-2\alpha r}}{\hbar^2(1-2\mathrm{e}^{-2\alpha r})^2}+\frac{4m_{\mathrm{e}}^*V_0}{\hbar^2}\cosh(\alpha r_0)\sinh(\alpha r_0)\frac{(1+\mathrm{e}^{-2\alpha r})}{(1-\mathrm{e}^{-2\alpha r})}$$
$$\left.-\frac{4\alpha^2l(l+1)\mathrm{e}^{-2\alpha \mathrm{r}}}{(1-\mathrm{e}^{-2\alpha r})^2}\right\}U_{nl}(r)=0. \tag{7}$$

With the change of variable $z=\mathrm{e}^{-2\alpha r}$, we have

$$\frac{\mathrm{d}^2U_{nl}(r)}{\mathrm{d}z^2}+\frac{(1-z)}{z(1-z)}\frac{\mathrm{d}U_{nl}(z)}{\mathrm{d}z}+\frac{1}{(z(1-z))^2}(Az^2+Bz+C)U_{nl}(z)=0. \tag{8}$$

The parameters A, B, and C are defined as

$$A=\frac{mE_{nl}}{2\alpha^2\hbar^2}-\frac{mV_0}{2\alpha^2\hbar^2}\cosh^2(\alpha r_0)-\frac{mV_0}{2\alpha^2\hbar^2}\sinh^2(\alpha r_0)$$
$$-\frac{mV_0}{2\alpha^2\hbar^2}\cosh(\alpha r_0)\sinh(\alpha r_0), \tag{9a}$$

$$B=\frac{mE_{nl}}{2\alpha^2\hbar^2}+\frac{mV_0}{2\alpha^2\hbar^2}\cosh^2(\alpha r_0)+\frac{mV_0}{2\alpha^2\hbar^2}\sinh^2(\alpha r_0)$$
$$-\frac{2mV_0}{2\alpha^2\hbar^2}\sinh^2(\alpha r_0)-l(l+1), \tag{9b}$$

$$C=\frac{mE_{nl}}{2\alpha^2\hbar^2}-\frac{mV_0}{2\alpha^2\hbar^2}\cosh^2(\alpha r_0)-\frac{mV_0}{2\alpha^2\hbar^2}\sinh^2(\alpha r_0)$$
$$+\frac{mV_0}{2\alpha^2\hbar^2}\cosh(\alpha r_0)\sinh(\alpha r_0). \tag{9c}$$

To solve eq. (8) and obtain eigenfunctions and eigenvalues, the Nikiforov–Uvarov (NU) technique is used [42–47]. First, consider the following equation:

$$\left\{\frac{\mathrm{d}^2}{\mathrm{d}s^2}+\frac{\alpha_1-\alpha_2s}{z\,(1-\alpha_3s)}\frac{\mathrm{d}}{\mathrm{d}s}+\frac{1}{(s\,(1-\alpha_3s))^2}\left(-\xi_1s^2+\xi_2s-\xi_3\right)\right\}\psi=0. \tag{10}$$

If the NU method is applied [47], the solutions of the above equation becomes

$$\psi(s)=s^{\alpha_{12}}(1-\alpha_3s)^{-\alpha_{12}-(\alpha_{13}/\alpha_3)}P_n^{(\alpha_{10}-1,(\alpha_{11}/\alpha_3)-\alpha_{10}-1)}(1-2\alpha_3s), \tag{11}$$

where

$$\begin{aligned}
\alpha_2 n \;&-\; (2n+1)\alpha_5 + (2n+1)(\sqrt{\alpha_9} + \alpha_3\sqrt{\alpha_8}) \\
&\quad + n(n+1)\alpha_3 + \alpha_7 + 2\alpha_3\alpha_8 + 2\sqrt{\alpha_8\alpha_9} = 0, \\
\alpha_4 \;&=\; \frac{1}{2}\left(1 - \alpha_1\right), \\
\alpha_5 \;&=\; \frac{1}{2}\left(\alpha_2 - 2\alpha_3\right), \\
\alpha_6 \;&=\; \alpha_5^2 + \xi_1, \\
\alpha_7 \;&=\; 2\alpha_4\alpha_5 - \xi_2, \\
\alpha_8 \;&=\; \alpha_4^2 + \xi_3, \\
\alpha_9 \;&=\; \alpha_3\alpha_7 + \alpha_3^2\alpha_8 + \alpha_6, \\
\alpha_{10} \;&=\; \alpha_1 + 2\alpha_4 + 2\sqrt{\alpha_8}, \\
\alpha_{11} \;&=\; \alpha_2 - 2\alpha_5 + 2\left(\sqrt{\alpha_9} + \alpha_3\sqrt{\alpha_8}\right), \\
\alpha_{12} \;&=\; \alpha_4 + \sqrt{\alpha_8}, \\
\alpha_{13} \;&=\; \alpha_5 - \left(\sqrt{\alpha_9} + \alpha_3\sqrt{\alpha_8}\right).
\end{aligned} \tag{12}$$

Now, by comparing eq. (8) with eq. (10), we get

$$\begin{aligned}
&\alpha_1 = 1, \quad \alpha_2 = 1, \quad \alpha_3 = 1, \quad \xi_1 = -A, \quad \xi_2 = B, \quad \xi_3 = -C, \\
&\alpha_4 = 0, \quad \alpha_5 = -\frac{1}{2}, \quad \alpha_6 = \xi_1 + \frac{1}{4}, \quad \alpha_7 = -\xi_2, \quad \alpha_8 = \xi_3, \\
&\alpha_9 = -\xi_2 + \xi_3 + \xi_1 + \frac{1}{4}, \quad \alpha_{10} = 1 + 2\sqrt{\xi_3}, \\
&\alpha_{11} = 2 + 2\left(\sqrt{-\xi_2 + \xi_3 + \xi_1 + \frac{1}{4}} + \sqrt{\xi_3}\right), \\
&\alpha_{12} = \sqrt{\xi_3}, \quad \alpha_{13} = -\frac{1}{4} - \left(\sqrt{-\xi_2 + \xi_3 + \xi_1 + \frac{1}{4}} + \sqrt{\xi_3}\right).
\end{aligned} \tag{13}$$

The energy levels of charge carriers are given by

$$\begin{aligned}
n + \frac{(2n+1)}{2} \;&+\; (2n+1)\left(\sqrt{-\xi_2 + \xi_3 + \xi_1 + \frac{1}{4}} + \sqrt{\xi_3}\right) + n\,(n-1) \\
&-\; \xi_2 + 2\xi_3 + 2\sqrt{-\xi_2\xi_3 + \xi_3^2 + \xi_1\xi_3 + \frac{\xi_3}{4}} = 0.
\end{aligned} \tag{14}$$

The wave functions are obtained as

$$\begin{aligned}
U_{nl}(r) = N_{nl}\mathrm{e}^{-2\alpha r\sqrt{\xi_3}}\left(1 - \mathrm{e}^{-2\alpha r}\right)^{\frac{1}{2} + \left(\sqrt{-\xi_2 + \xi_2 + \xi_1 + \frac{1}{4}}\right)} \\
\times\, P_n^{\left(2\sqrt{\xi_3, 2}\sqrt{-\xi_2 + \xi_3 + \xi_1 + \frac{1}{4}}\right)}\left(1 - 2\mathrm{e}^{-2\alpha r}\right),
\end{aligned} \tag{15}$$

$$P_n^{(K,L)} = \frac{\Gamma(n+1+K)}{n!\Gamma(1+K)}\,{}_2F_1(-n, n+K+L+1; K+1; xt). \tag{16}$$

Here $P_n^{(K,L)}$ is the associated Legendre polynomial. Inserting the above function in eq. (15), the wave functions can be written as

$$U_{nl}(r) = \mathrm{e}^{-2\alpha r\sqrt{\xi_3}}\left(1-\mathrm{e}^{-2\alpha r}\right)^{\frac{1}{2}+\left(\sqrt{-\xi_2+\xi_3+\xi_1+\frac{1}{4}}\right)} \times P_n^{\left(2\sqrt{\xi_3},2\sqrt{-\xi_2+\xi_3+\xi_3+\frac{1}{4}}\right)}\frac{\Gamma(n+1+2\sqrt{\xi_3})}{n!\Gamma(1+2\sqrt{\xi_3})} \times {}_2F_1\left(-n, n+2\sqrt{\xi_3}+2\sqrt{-\xi_2+\xi_3+\xi_1+\frac{1}{4}}+1; 2\sqrt{\xi_3}+1; \mathrm{e}^{-2\alpha r}\right). \quad (17)$$

3. Optical absorption coefficients and refractive index changes

In this section, the optical properties are calculated using the density matrix method [48,49]. It is known that the system under study can be excited by an electromagnetic field of frequency ω such that

$$E(t) = E_0\cos(\omega t) = \tilde{E}\mathrm{e}^{i\omega t} + \tilde{E}^*\mathrm{e}^{-i\omega t}. \quad (18)$$

The time evolution of the matrix elements of one-electron density operator, ρ, can be written as [50,51]

$$\frac{\partial\rho}{\partial t} = \frac{1}{i\hbar}\left[H_0 - qxE(t), \rho\right] - \Gamma(\rho-\rho^{(0)}), \quad (19)$$

where H_0 is the Hamiltonian for this system without the electromagnetic field $E(t)$, q is the electronic charge. The symbol [,] is the quantum mechanical commutator, $\rho^{(0)}$ is the unperturbed density matrix operator, and Γ is the phenomenological operator responsible for the damping due to the electron–phonon interaction, collisions among electrons, etc. It is assumed that Γ is a diagonal matrix and its elements are equal to the inverse of relaxation time T. Equation (20) can be solved using the standard iterative method [52]:

$$\rho(t) = \sum_n \rho^{(n)}(t) \quad (20)$$

with

$$\frac{\partial\rho_{ij}^{(n+1)}}{\partial t} = \frac{1}{i\hbar}\left\{\left[H_0, \rho^{(n+1)}\right]_{ij} - i\hbar\Gamma_{ij}\rho_{ij}^{(\pi n+1)}\right\} - \frac{1}{i\hbar}\left[qx\cdot\rho^{(n)}\right]_{ij}E(t). \quad (21)$$

For simplicity, we shall only focus on two-level electronic systems for electronic transitions. Therefore, the electronic polarization $P(t)$ and susceptibility $\chi(t)$ are expressed by dipole operator M and density matrix ρ

$$P(t) = \varepsilon_0\chi(\omega)\tilde{E}\mathrm{e}^{-i\omega t} + \varepsilon_0\chi(-\omega)\widetilde{E^*}\mathrm{e}^{i\omega t} = \frac{1}{V}\mathrm{Tr}(\rho M), \quad (22)$$

where ρ and V are the one-electron density matrix and the volume of the system, ε_0 is the permittivity of free space, and the symbol Tr (trace) denotes the summation over the diagonal elements of the matrix.

The analytical forms of the linear $\chi^{(1)}$ and the third-order nonlinear $\chi^{(3)}$ susceptibility coefficients are obtained from eqs (21) and (22) as

$$\varepsilon_0\chi^{(1)}(\omega) = \frac{\sigma_v|M_{21}|^2}{E_{21} - \hbar\omega - i\hbar\Gamma_{12}}, \tag{23}$$

$$\varepsilon_0\chi^{(3)}(\omega) = -\frac{\sigma_v|M_{21}|^2|E|^2}{E_{12} - \hbar\omega - i\hbar\Gamma_{12}}\left[\frac{4|M_{21}|^2}{(E_{12} - \hbar\omega)^2 - (\hbar\Gamma_{12})^2} - \frac{(M_{22} - M_{11})^2}{(E_{21} - i\hbar\Gamma_{12})(E_{12} - \hbar\omega - i\hbar\Gamma_{12})}\right], \tag{24}$$

where σ_v is the carrier density. The changes in refractive index are related to the susceptibility as [39]

$$\frac{\Delta n^{(1)}(\omega)}{n_r} = \mathrm{Re}\left(\frac{\chi(\omega)}{2n_r^2}\right), \tag{25}$$

where n_r is the refractive index. By using eqs (22)–(24), the linear and the third-order nonlinear refractive index changes can be expressed as [24]

$$\frac{\Delta n^{(1)}(\omega)}{n_r} = \frac{1}{2n_r^2\varepsilon_0}|M_{21}|^2\sigma_v\left[\frac{E_{21} - \hbar\omega}{(E_{12} - \hbar\omega)^2 + (\hbar\Gamma_{12})^2}\right] \tag{26}$$

and

$$\frac{\Delta n^{(3)}(\omega)}{n_r} = -\frac{\mu c}{4n_r^2\varepsilon_0}|M_{21}|^2\frac{\sigma_v I}{\left[(E_{12} - \hbar\omega)^2 + (\hbar\Gamma_{12})^2\right]^2} \times \left\{4(E_{21} - \hbar\omega)|M_{21}|^2 - \frac{(M_{22} - M_{11})^2}{(E_{21})^2 + (\hbar\Gamma_{12})^2} \times [(E_{21} - \hbar\omega)\{E_{21}(E_{21} - \hbar\omega) - (\hbar\Gamma_{12})^2\} - (\hbar\Gamma_{12})^2(2E_{21} - \hbar w)]\right\}, \tag{27}$$

where μ is the permeability, $E_{ij} = E_i - E_j$, and $M_{ij} = \left|\langle\varphi_i\left|qx\right|\varphi_j\rangle\right|$ is the electric dipole moment matrix element. In this work, the polarization of the electric field in z direction is selected.

The symbol I is the optical intensity of the incident wave and it is expressed as

$$I = 2\sqrt{\frac{\varepsilon_R}{\mu}}|E(\omega)|^2 = \frac{2n_r}{\mu c}, \tag{28}$$

where c is the speed of light in free space. Using eqs (27) and (28), one can write the change in total refractive index as

$$\frac{\Delta n(\omega)}{n_r} = \frac{\Delta n^1(\omega)}{n_r} + \frac{\Delta n^3(\omega)}{n_r}. \tag{29}$$

The susceptibility $\chi(\omega)$ is related to the absorption coefficient $\alpha(\omega)$ and real part of permittivity as

$$\alpha(\omega) = \omega\sqrt{\frac{\mu}{\varepsilon_R}}\mathrm{Im}[\varepsilon_0\chi(\omega)]. \tag{30}$$

Now, the linear and third-order nonlinear absorption coefficients can be written as [52]

$$\alpha^1(\omega) = \omega\sqrt{\frac{\mu}{\varepsilon_R}}\left[\frac{\sigma_v\hbar\Gamma_{12}|M_{21}|^2}{(E_{12}-\hbar\omega)^2+(\hbar\Gamma_{12})^2}\right], \tag{31}$$

$$\begin{aligned}\alpha^3(\omega,\ I) = &\left(-\omega\sqrt{\mu/\varepsilon_R}\left(\frac{I}{2\varepsilon_0 n_r C}\right)\frac{|M_{21}|^2\sigma_v\hbar\Gamma_{12}}{\left[(E_{21}-\hbar\omega)^2+(\hbar\Gamma_{12})^2\right]^2}\right)\\ &\times 4\,|M_{21}|^2\\ &\times\left[\frac{|M_{22}-M_{11}|^2\left[3E_{21}^2-4E_{21}\hbar\omega+\hbar^2\left(\omega^2-\Gamma_{12}^2\right)\right]}{E_{21}^2+\left(\hbar\Gamma_{12}^2\right)}\right].\end{aligned} \tag{32}$$

Using eqs (32) and (33), one can express the total absorption coefficient $\alpha(\omega, I)$ as [24]

$$\alpha(\omega, I) = \alpha^1(\omega) + \alpha^3(\omega, I). \tag{33}$$

4. Results and discussions

In this section, we choose GaAs as an example to present the numerical results. In our calculations, the following parameters are used: $I = 0.2\,\mathrm{MW/cm^2}$, $\varepsilon_0 = 8.85\times10^{-12}$ F·m^{-1}, $\alpha = 0.01$, $m = 5$ fm^{-1}, $r_0 = 2$, $\hbar = 1$, and $v_0 = 0.2, 0.4, 0.6, 0.8$. It is worth mentioning that the effective Bohr radius and the effective Rydberg are length and energy scales, respectively.

In figure 1, the linear, third-order nonlinear, and total refractive index changes are plotted as functions of the photon energy for $\alpha = 0.01$, $m = 5$ fm^{-1}, $r_0 = 2$, and $v_0 = 0.2$. It is to be noted that the change in third-order nonlinear refractive index is negative and therefore the change in total refractive index will be reduced. Also, the larger change in the total refractive index is mainly caused by the linear term which is much larger than nonlinear term with the opposite sign. For systems operating with a high optical intensity, the calculation of the change in refractive index using only the linear term, may be excessively optimistic.

Figure 2 displays the change in total refractive index as a function of photon energy for $v_0 = 0.2, 0.4, 0.6$, $\alpha = 0.01$, $m = 5$ fm^{-1}, and $r_0 = 2$. It is seen from the figure that the change in total refractive index increases and also shifts toward higher energies when v_0 increases. The physical origin of this increases is the quantum confinement effect which predicts a strong confinement in the quantum dot when v_0 enhances. Also, the energy level spacing increases when v_0 increases. For this reason, the changes in total refractive index shift towards higher energies.

In figure 3, the changes in total refractive index as a function of photon energy with $\alpha = 0.01$, $m = 5$ fm^{-1}, and $v_0 = 2$ for $r_0 = 2$, 3, and 4 have been presented. It can be seen that as r_0 increases, the total refractive index shifts toward lower energies. The

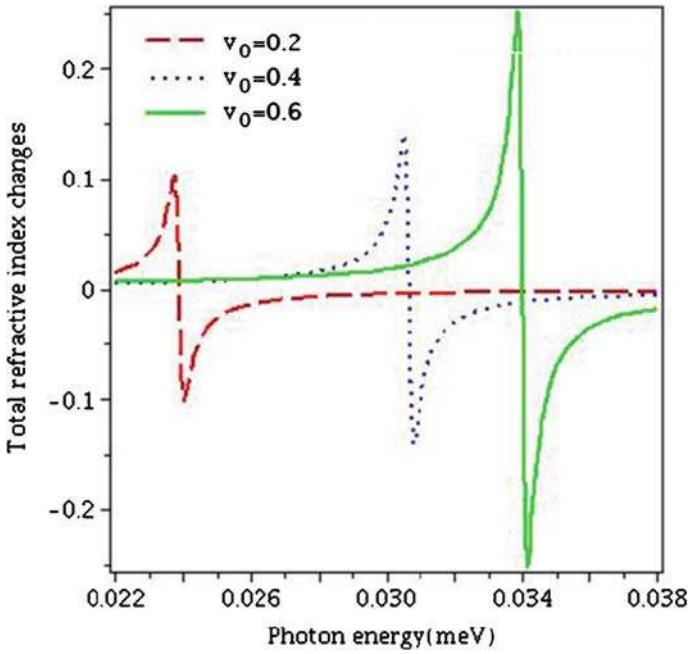

Figure 2. The changes in total refractive index as functions of photon energy for three different v_0 with $\alpha = 0.01$, $m = 5$ fm^{-1}, and $r_0 = 2$.

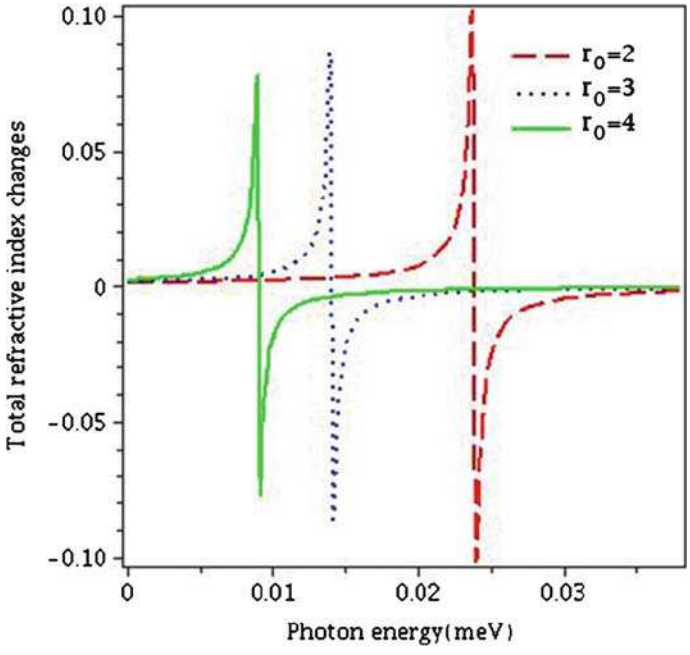

Figure 3. The changes in total refractive index as functions of photon energy for three different r_0 with $\alpha = 0.01$, $m = 5$ fm^{-1}, and $v_0 = 0.2$.

physical reason for this shift is the decrease in energy gap of two different electronic states, $E_2 - E_1$, between which an optical transition occurs. Also, by increasing r_0, the quantum confinement effect decreases.

Figure 4 shows the linear, third-order nonlinear, and total absorption coefficients as a function of photon energy for $\alpha = 0.01$, $m = 5$ fm^{-1}, $r_0 = 2$, and $v_0 = 2$. In this figure, there is a resonance peak at a photon energy of 0.2 meV as expected, which relates to the energy difference between the levels considered. It is clear that the third-order nonlinear absorption coefficient is negative and therefore reduces the total absorption coefficient. Also, the larger change in total absorption coefficient is mainly caused by the linear term which is much larger than the nonlinear term with the opposite sign for relatively low intensity.

In figure 5, the variations of total absorption coefficient are plotted as a function of photon energy for $v_0 = 0.2, 0.4, 0.6$ with $\alpha = 0.01$, $m = 5$ fm^{-1}, and $r_0 = 2$. It is observed from the figure that the total absorption coefficient reduces and shifts towards higher energies as v_0 increases. The reason for this behaviour is the increase in quantum confinement with increased v_0. Also, the energy level spacing increases with increasing v_0.

In figure 6, the total absorption coefficient has been plotted as a function of photon energy with $\alpha = 0.01$, $m = 5$ fm^{-1}, and $v_0 = 0.2$ for $r_0 = 2$, 3, and 4. It can be seen that as r_0 decreases, the total absorption coefficients shift toward higher energies. The physical reason for this shift is the increase in energy gap of two different electronic states, $E_2 - E_1$, between which an optical transition occurs. Also, by increasing r_0, the quantum confinement effect decreases.

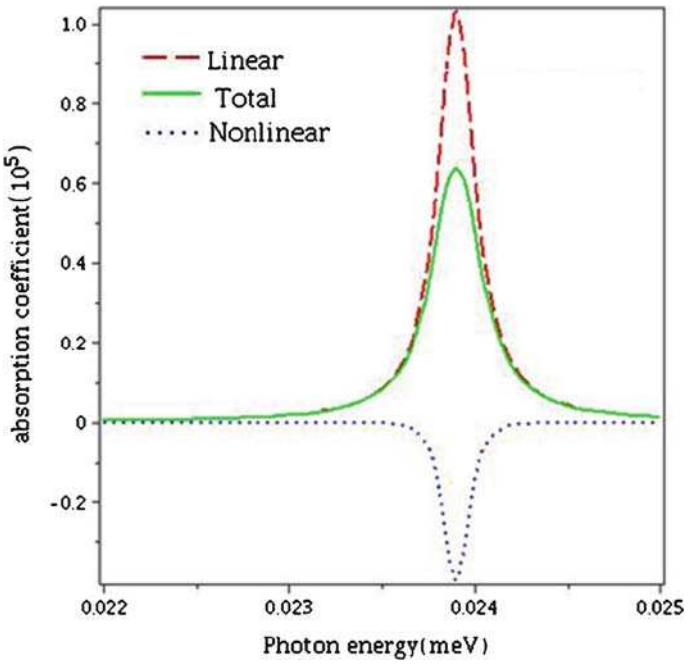

Figure 4. The linear, third-order nonlinear, and total absorption coefficient as a function of photon energy for $\alpha = 0.01$, $m = 5$ fm^{-1}, $r_0 = 2$, and $v_0 = 0.2$.

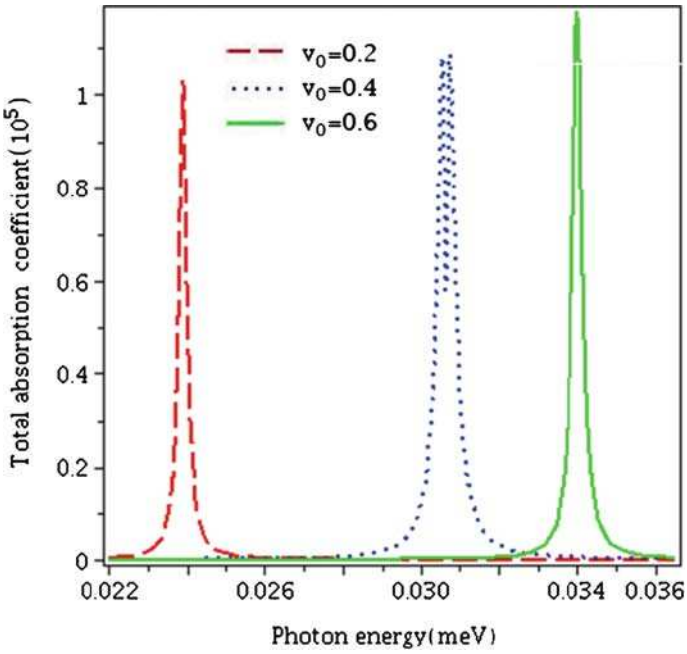

Figure 5. The total absorption coefficient as a function of photon energy for three different v_0 with $\alpha = 0.01$, $m = 5$ fm^{-1}, and $r_0 = 2$.

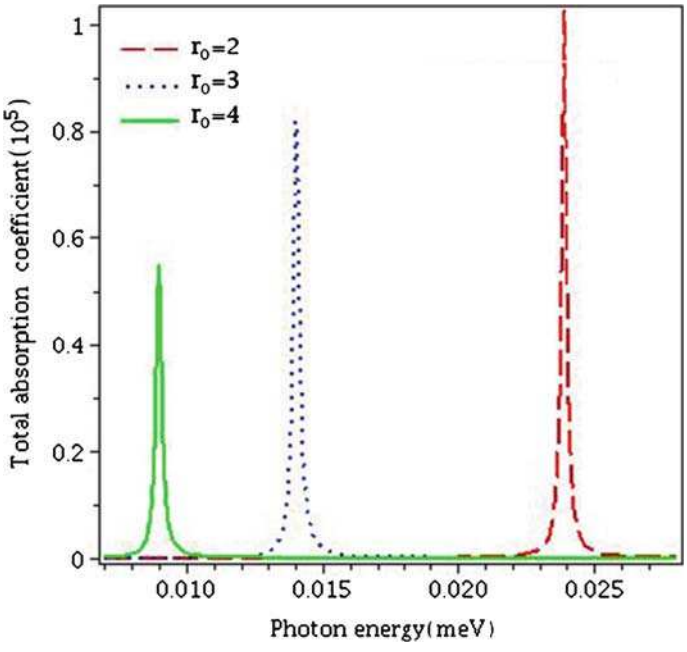

Figure 6. The total absorption coefficient as a function of photon energy for three different r_0 with $\alpha = 0.01$, $m = 5$ fm^{-1}, and $v_0 = 0.2$.

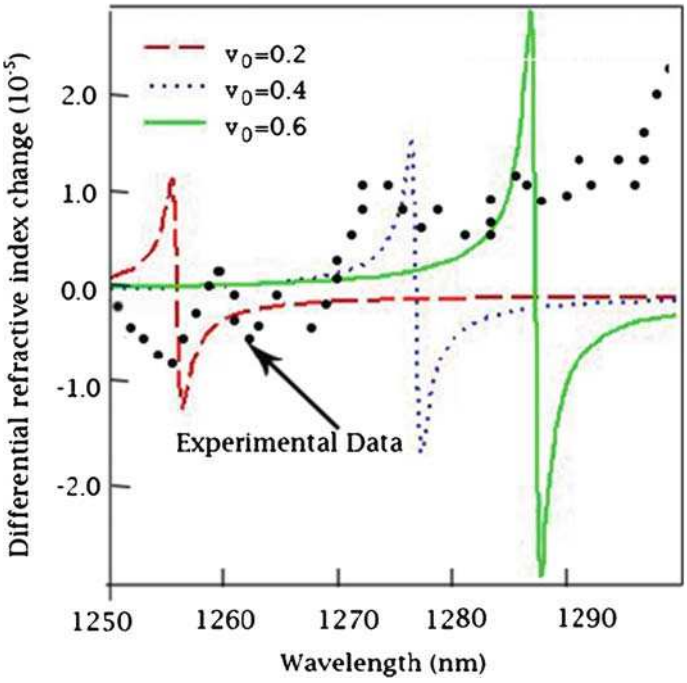

Figure 7. Differential refractive index changes (Δn) as a function of photon wavelength for three different v_0 with $\alpha = 0.01$, $m = 5$ fm^{-1}, and $r_0 = 2$. In this figure, we have compared our results with the experimental data (filled circles) of [52].

Figure 7 shows differential refractive index changes (Δn) as a function of photon wavelength for $v_0 = 0.2, 0.4, 0.6$ with $\alpha = 0.01$, $m = 5$ fm^{-1}, and $r_0 = 2$, and $I = 0.3$ mW. We have presented the experimental data [53] and compared with our results. From the figure, one can see that our theoretical prediction deviates from the experimental data [53]. Related to this deviation, several points should be noted: (i) Considering the two-level system for electronic transitions is not perfectly exact. (ii) There are several parameters in our calculations like v_0, r_0, σ_v, and I which may be temperature-dependent. The determination of potential parameters is difficult. But, we have considered these parameters as independent of temperature. (iii) All calculations have been performed by numerical methods but these methods often show some errors. (iv) The potential model used in this work may not be a good one for calculating optical properties. To understand it further, the reader can refer to the experimental results [54–56].

5. Conclusions

In this work, we have studied theoretically the linear, third-order nonlinear, and total absorption coefficients, and the changes in refractive index for a spherical quantum dot. For this purpose, we have applied the Tietz potential as quantum confinement. We have solved the Schrödinger equation and obtained energy levels and wave functions. Then,

using the density matrix method, we have studied the optical properties. The obtained results show that the absorption coefficients and changes in refractive index increase and shift towards higher energies as v_0 increases. With increasing r_0, the absorption coefficients and changes in refractive index decrease and shift towards lower energies. In general, structure parameters v_0 and r_0 have important roles in the absorption coefficients and refractive index changes.

References

[1] G Schmid (ed.), *Clusters and colloids, from theory to applications* (VCH, New York, 1994)
[2] M A Kastner, *Phys. Today* **46**, 24 (1993)
[3] R Khordad and B Mirhosseini, *Physica B* **408**, 10 (2013)
[4] D Bimberg, M Grundman and N Ledentsov, *Quantum dot heterostructures* (Wiley, New York, 1999)
[5] N Miura, *Physics of semiconductors in high magnetic fields* (Oxford University Press, New York, 2008)
[6] H M Gibbs, *Optical bistability: Controlling light with light* (Academic Press, Orlando, NY, 1985)
[7] R Khordad, *J. Lumin.* **134**, 201 (2013)
[8] S Hosseynizadeh Khezri, A Yazdani and R Khordad, *Eur. Phys. J. Appl. Phys.* **59**, 30401 (2012)
[9] R Khordad and H Bahramiyan, *Int. J. Mod. Phys. C* **24**, 1350041 (2013)
[10] D A Neamen, *Semiconductor physics and devices* 3rd edn (McGraw-Hill, 2003)
[11] S D Liang, C Y Chen, S C Jiang and D L Lin, *Phys. Rev. B* **53**, 15459 (1996)
[12] U Bockelmann and G Bastard, *Phys. Rev. B* **42**, 8947 (1990)
[13] V M Fomin, V N Gladilin, S N Klimin, J T Devreese, P M Koenraad and J H Wolter, *Phys. Rev. B* **61**, R2436 (2000)
[14] R Heitz, I Mukhametzhanov, O Stier, A Madhukar and D Bimberg, *Phys. Rev. Lett.* **83**, 4654 (1999)
[15] K-X Guo and C-Y Chen, *Tr. J. Phys.* **21**, 1261 (1997)
[16] R Khordad, *Superlatt. Microstruct.* **54**, 7 (2013)
[17] W Dieter Heiss, *Quantum dots (A doorway to nanoscale physics)* (Springer, 2005)
[18] G Wang and Q Guo, *Physica B* **403**, 37 (2008)
[19] R Khordad, *Opt. Quant. Electron.* **46**, 283 (2014)
[20] S Shao, K X Guo, Z H Zhang, N Li and C Peng, *Superlatt. Microstruct.* **48**, 541 (2010)
[21] A L Morales, N Raigoza and C A Duque, *Braz. J. Phys.* **36**, 862 (2006)
[22] I Karabulut and S Baskoutas, *J. Comput. Theoret. Nanosci*. **6**, 153 (2009)
[23] R Khordad, S Kheiryzadeh Khaneghah and M Masoumi, *Superlatt. Microstruct.* **47**, 538 (2010)
[24] R Khordad and B Mirhosseini, *Opt. Commun.* **285**, 1233 (2012)
[25] H Nikoofard, E Maghsoodi, S Zarrinkamar, M Farhadi and H Hassanabadi, *Turk. J. Phys.* **37**, 74 (2013)
[26] P M Morse, *Phys. Rev.* **34**, 57 (1929)
[27] N Rosen and P M Morse, *Phys. Rev*. **42**, 210 (1932)
[28] H Wei, *Phys. Rev. A* **42**, 2524 (1990)
[29] T Tietz, *J. Chem. Phys.* **35**, 1917 (1961)
[30] A A Zavitsas, *J. Am. Chem. Soc.* **113**, 4755 (1991)
[31] P G Hajigeorgious and R J Le Roy, *J. Chem. Phys.* **112**, 3949 (2000)
[32] Y Huang and R J Le Roy, *J. Chem. Phys.* **119**, 7398 (2003)

[33] H M Tang, G C Liang, L H Zhang, F Zhao and C S Jia, *Can. J. Chem.* **92**, 201 (2014)
[34] R T Pack, *J. Chem. Phys.* **57**, 4612 (1972)
[35] G C Liang, H M Tang and C S Jia, *Comput. Theor. Chem.* **1020**, 170 (2013)
[36] R Khordad and B Mirhosseini, *Commun. Theor. Phys.* **62**, 77 (2014)
[37] Y Sun, S He and C S Jia, *Phys. Scr*. **87**, 025301 (2013)
[38] C S Jia, T Chen, L Z Yi and S R Lin, *J. Math. Chem.* **51**, 2165 (2013)
[39] X T Hu, J Y Liu and C S Jia, *Comput. Theor. Chem.* **1019**, 137 (2013)
[40] H Hassanabadi, E Maghsoodi and S Zarrinkamar, *Eur. Phys. J. Plus* **127**, 31 (2012)
[41] W C Qiang and S H Dong, *Phys. Lett. A* **368**, 13 (2007)
[42] H Hassanabadi, E Maghsoodi, S Zarrinkamar and H Rahimov, *J. Math. Phys.* **53**, 022104 (2012)
[43] M G Miranda, G H Sun and S H Dong, *Int. J. Mod. Phys. E* **19**, 123 (2010)
[44] M C Zhang, G H Sun and S H Dong, *Phys. Lett. A* **374**, 704 (2010)
[45] G H Sun and S H Dong, *Mod. Phys. Lett. A* **25**, 2849 (2010)
[46] F Nikiforov and V B Uvarov, *Special functions of mathematical physics* (Birkhauser, Basel, 1988)
[47] A Berkdemir and J H Berkdemir, *Chem. Phys. Lett.* **417**, 326 (2006)
[48] E Rosencher and P Bois, *Phys. Rev. B* **44**, 11315 (1991)
[49] T Takagahara, *Phys. Rev. B* **36**, 9293 (1987)
[50] G H Wang, Q Guo and K X Guo, *Chin. J. Phys.* **41**, 296 (2003)
[51] S Ünlü, I Karabulut and H Safak, *Physica E* **33**, 319 (2006)
[52] D Ahn and S L Chuang, *IEEE J. Quant. Electron.* **23**, 2196 (1987)
[53] J Kim and S L Chuang, *IEEE J. Quant. Electron.* **42**, 942 (2006)
[54] I Moreels, P Kockaert, D V Thourhout and Z Hens, *Proceedings Symposium IEEE/LEOS Benelux Chapter* (Brussels, 2007)
[55] J Chen, X Chen, R Xu, Y Zhu, Y Shi and X Zhu, *Solid State Commun.* **281**, 3578 (2008)
[56] Y Takahashi, Y Hayamizu, H Itoh, M Yoshita, H Akiyama, L N Pfeiffer and K W West, arXiv:0502363v1 (2005)